



Experimental and stochastic analysis of lyophilisation

J. Ravnik, M. Ramšak, M. Zadavec, B. Kamenik, M. Hriberšek*

Faculty of Mechanical Engineering, University of Maribor, Smetanova ulica 17, SI-2000 Maribor, Slovenia

ARTICLE INFO

Keywords:

Freeze-drying
Stochastic collocation method
Boundary element method
Uncertainty analysis
Lyophilization

ABSTRACT

The development of the freeze-drying processes through the use of a combination of targeted experiments and the application of multidimensional computational models is applied increasingly in pharmaceutical practice, especially for scale-up purposes. This study deals with the analysis of uncertainties in the data on material properties and model parameters, and their influence on the results delivered by advanced computational models of lyophilisation. As a means of uncertainty analysis, the Stochastic Collocation Method is applied, allowing the use of existing reliable deterministic models as black boxes in the stochastic computations. As a deterministic model, the lyophilisation model is used, based on the axisymmetric approximation of a vial, and the Boundary Element Method as a solver. Five parameters, covering material properties, process conditions and model constants, are selected for the sensitivity analysis simulation of the lyophilisation of an aqueous mannitol solution. The results show that during the initial stage of the primary drying heat transfer from the shelf is crucial, and that the uncertainties in the contact surface area and material properties of the vial play a more important role than the thermal properties of the drying material. When the temperature of the material reaches its distinct primary drying stage level the mass transfer through the porous cake becomes the most important, with great sensitivity to the Knudsen diffusivity in the porous cake. We observed uncertainties in the results for the primary drying time in the order of $\pm 6\%$, and uncertainties in the results for temperatures of $\pm 0.6^\circ\text{C}$ in the frozen material and $\pm 3^\circ\text{C}$ in the porous cake. The uncertainty analysis proved to be a great help in determining the critical parameters in the heat and mass transfer during the important primary drying step, which led to a better definition of the numerical model for use in the context of design space determination.

1. Introduction

The processes of separation of a solvent from a solid–liquid mixture are commonly required in Pharmaceutical Engineering, the food industry and Materials Science. One of the possibilities is drying, which is, typically, a highly energy intensive process, which can, in the case of pharmaceutical implementations, present problems in the degradation of formulation properties. A thermally gentle variation of drying is lyophilisation, consisting of a freezing step, in which the initially liquid formulation is frozen, followed by the freeze drying step, in which a sublimation driven mass transfer of frozen solvent from the solid to the vapour phase separates the solid formulation constituents from the solvent phase. The freeze drying step consists of the primary drying phase, where the frozen solvent is removed, followed by the secondary drying step, where the solvent adsorbed on the remaining solid phase of the formulation is removed in a process of desorption. A typical lyophilisation device consists of a vacuum chamber, where the product is

placed on cooled/heated shelves. As the lyophilisation is energy intensive, optimisation of the drying protocol is needed, i.e. the set-up of the shelf temperatures in the primary and secondary drying phases, as well as system pressure. In recent years, a combination of targeted experiments and the use of validated computational models based on the use of lyophilisation mechanistic models [1], already showed promise as an efficient procedure for optimisation of the drying conditions i.e. design space determination [2–4]. The computational part of the used models is based on the fundamental understanding of the process under study, as well as on the underlying physical mechanisms of heat and mass transfer, [5–10], and presents a powerful tool for both lyophilisation cycle development and design space determination. Although implementation of deterministic numerical techniques based on the mechanistic models led to a good insight into the behaviour of the underlying phenomena, there are still some problems that cannot be solved by deterministic modelling alone. The mathematical-physical model describing the lyophilisation processes is based on the material

* Corresponding author.

E-mail addresses: jure.ravnik@um.si (J. Ravnik), matjaz.ramsak@um.si (M. Ramšak), matej.zadavec@um.si (M. Zadavec), blaz.kamenik@um.si (B. Kamenik), matjaz.hribersek@um.si (M. Hriberšek).

<https://doi.org/10.1016/j.ejpb.2020.12.011>

Received 8 September 2020; Received in revised form 27 November 2020; Accepted 12 December 2020

Available online 30 December 2020

0939-6411/© 2020 Elsevier B.V. All rights reserved.

parameters and model parameters which are some predetermined, mostly averaged, values of the real material and the correct model values. When used in computational models, these average values lead to computational results, that are an approximation of the realistic situation. Each process is sensitive to a change in process conditions, and if there is an additional sensitivity to the material and model parameters used in the computational model, the uncertainty from the input will inevitably be transferred to the output of interest, which are, in the case of lyophilisation, the temperature and moisture distribution in the dried material. In order to get a better insight into the quality of computational results, the model input parameters should be considered as random variables, and an appropriate computational uncertainty analysis should be performed. Recently, the use of non-deterministic approaches in computational analysis of lyophilisation design space has been reported, [11,12]. Traditionally, Monte Carlo type methods have been used to capture the response of deterministic simulations to changes in input parameters. These methods have an extremely slow convergence rate, which means that a very large number of deterministic simulations are required to obtain statistically relevant results. In the case of physically and numerically more sophisticated models, of which Computational Fluid Dynamics is a prime example, it is not possible to perform a very large number of simulations. In contrast to statistical approaches, the non-statistical algorithms aim to represent the unknown stochastic solution as a function of random input variables. Among the different methods available in the literature, the Generalized Polynomial Chaos (gPCE) technique, based on spectral discretisation, is one of the most commonly used. Two variants of gPCE are the Galerkin Stochastic Method (SGM) and Stochastic Collocation Method (SCM) [13]. The intrusive nature of the SGM requires a more sophisticated implementation, as new algorithms have to be developed. On the contrary, the non-intrusive nature of SCM allows the use of existing reliable deterministic models, such as black boxes in stochastic computations. Both approaches show fast convergence and high accuracy under different conditions, and a detailed comparison of their use can be found in [14]. The combination of the non-intrusive, sample-based character of Monte Carlo simulations with the polynomial approximation of the output value, which is characteristic of gPCE methods, made stochastic collocation one of the most researched and applied stochastic approaches [15–17]. With further development of modelling approaches in the study of lyophilisation, several studies have been conducted and reported on the computational analysis of uncertainties in parameter estimates and its influence on computed target values. A risk assessment based study of the freeze-drying cycle for pharmaceutical and its use in design space determination is reported in [18], with the monodimensional (0D) lyophilisation model used to compute the temperature at the bottom of the vial, followed by the calculation of the probabilistic distribution of the product temperature. In [11,12], the sampling-based method approach is used for evaluation of uncertainties in model predictions based on a 0D mechanistic lyophilisation model, with quantitative estimation of the risk of cake collapse using the mechanistic model. The definitive screening design was applied in the work of [19], with a focus on interactions between formulation and process parameters, which can be applied in early phase lyophilisation development strategy. Recently, a sensitivity study of the robustness of the primary drying with respect to the deviations in process parameters, using a generalised Polynomial Chaos method with Smolyak interpolation, was reported in [20]. In this paper we present the Boundary Element Method (BEM) based deterministic simulation solver for freeze drying processes, and validate it by experimental measurements. In addition, we couple the BEM solver with the Stochastic Collocation Method to account for the uncertainties present in the model's input parameters. The result is an analysis of the significance and uncertainties associated with the design parameters for freeze drying. This is of paramount importance when designing new freeze dryers, or to create new drying protocols for new substances. The paper is organised as follows: The experimental apparatus and measurements are presented in Section 2. This is followed

by the description of the BEM based deterministic solver and the mathematical model of the freeze drying process used. In Section 4 the SCM is developed, and its coupling to the BEM solver explained. In Section 5 we present the results, focusing on the relative importance of input parameters and their influence on the simulation results and the consequence for the design process of freeze dryers.

2. Experiment

When setting up the lyophilisation numerical model the first step is to perform several targeted experimental runs of the considered formulation under typical process conditions. Based on the results of experiments, typically in the form of a time series of measured temperatures in the product, or a combination of recorded temperatures and mass flow rates [21], model parameters are determined, and the corresponding numerical model validated. The experimental set-up, as well as results used for validation of the numerical model, are presented in the following.

2.1. Materials

The experiments were performed with 10 ml Schott 6R borosilicate glass vials. The outer diameter of the vial used in the experiment was 22 mm and the inner 20 mm. The vials were filled with a 4 g of 5% W/w aqueous mannitol solution as a model solution, as mannitol is used frequently as a crystalline bulking agent, providing the cake with a stronger structure and helping to maintain the physical stability of the pharmaceutical product [22,23]. Distilled water was used as the solvent.

2.2. Freeze-dryer

The freeze dryer was manufactured by the Kambic company [24]. The dryer has a separate drying chamber with two temperature regulated stainless steel shelves, each with a shelf area of about 0.09 m², and a condensation chamber with condenser capacity of 5 kg. The shelf temperature during the experiment varied between –35 °C and +10 °C and temperature of condenser was set to –86 °C. The chamber pressure was measured with a Pirani gauge, which was also used to regulate the vacuum pump. The measuring principle of the Pirani gauge is based on measuring the thermal conductivity of the gas, which depends on the gas' composition. If water vapour is present, the measured values are higher, due to the different thermal conductivity of the gases. Therefore, the system pressure set-up used to perform the experimental tests was determined using a ratio of 1.5 between the Pirani and capacitance sensors [25]. The main focus of this investigation is the primary drying phase, during which the gas composition within the chamber consists mainly of water vapour. The assumption to use the ratio between the Pirani and the capacitance sensor to determine the system pressure becomes questionable towards the end of the primary drying phase, because the gas composition within the chamber changes from mainly water vapour to inert gas, due to the lower water vapour mass flow. This means that the pressure readings of the Pirani gauge become more accurate, and the pressure in the chamber effectively rises, influencing the heat transfer rate, as well as the pressure difference in the last part of the primary drying. As the Pirani sensor readings were not used to determine the end of the primary drying, and in view of the findings presented in this paper that the system pressure sensitivity to observed process parameters is low compared to some other influencing parameters in the predictive computational model, the use of the constant pressure ratio factor for the primary drying phase does not present a major impact on the analysis of the results. On the other hand, to measure the product temperature, the dryer was also equipped with 7 thermocouples of type T, which were 0.5 mm thick. The data were collected using the National Instrument NI cDAQ-9174 system.

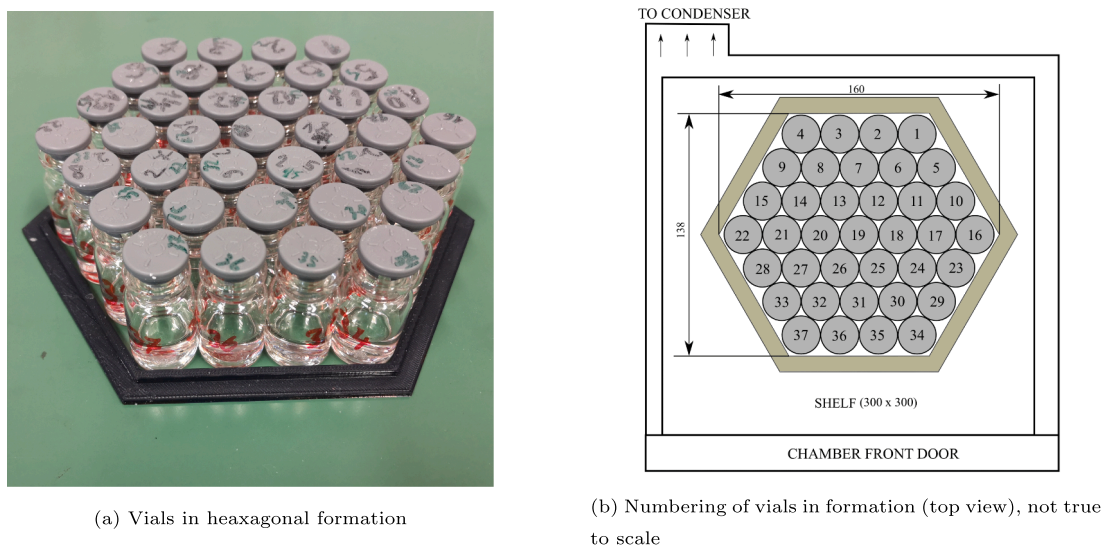


Fig. 1. Placement of vials on the shelf of the freeze-dryer.

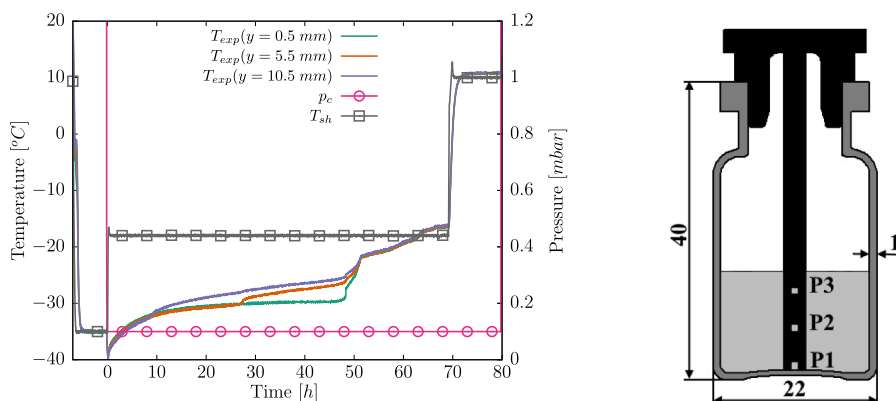


Fig. 2. Time trace of shelf temperature T_{sh} (left) with typical thermocouple readings at selected positions in the central vial 19. p_c is the chamber pressure measured by the Pirani pressure gauge. Vial cross-section with thermocouple positions is shown in the right panel.

2.3. Experiment protocol

Since the purpose of the experiment was to determine the drying kinetics of the centre vial, a total of 37 vials with half inserted rubber stoppers were used, placed in a hexagonal packing array, with the vial on position 19 in the centre of the shelf (Fig. 1a). The packing array was arranged using a 3D printed vial holder, with vial numbering and their relative positions with respect to the interior of the drying chamber shown in Fig. 1b. Before every measurement the vials were filled with 4 g of 5% W/w aqueous mannitol solution. After filling, every vial was weighed and placed in its corresponding position in the formation. Vials were then inserted onto the bottom shelf, while the top shelf was not loaded. In order to limit the heat gains from the surroundings, arising due to the front plexi glass observation doors, the front door was insulated with a 2 cm thick styrodur plate. After each measurement vials were emptied, washed and dried. In order to limit the effect of the ice buildup on the condenser surfaces, the condenser was defrosted completely before each experimental run. The freezing phase lasted for 7 h at the shelf temperature T_{sh} of $-35\text{ }^\circ\text{C}$ and atmospheric pressure. This was followed by the primary drying phase at the shelf temperature of $-18\text{ }^\circ\text{C}$ and the chamber pressure of $p_c = 10\text{ Pa}$, regulated by the Pirani pressure gauge. Consequently, we estimated the system pressure at $p_{syst} = p_c/1.5 = 6.67\text{ Pa}$. This was followed by the secondary drying

at the same pressure and shelf temperature of $+10\text{ }^\circ\text{C}$, see protocol for shelf temperature and chamber pressure in Fig. 2.

2.4. Measurement of temperatures inside of the vial

The temperatures were measured in vials at locations 18, 19 (centre vial) and 20. To limit the influence of the geometry of the thermocouple holder on the process, the holder was designed to mimic the rubber stopper geometry with an additional thermocouple positioning rod. The positioning rod had three positioning holes, P1-P3, through which the thermocouples were inserted. The holder was 3D printed, and ensured that the thermocouples were positioned at three heights: The first at the bottom of the vial (height = $0.5 \pm 0.5\text{ mm}$), the second at $5.5 \pm 0.5\text{ mm}$ above the bottom, and the third at $10.5 \pm 0.5\text{ mm}$ above the bottom. The typical temperature dynamics of the measurements at different heights in a vial is shown in Fig. 2.

2.5. Measurement of mass

The main focus in the experimental tests was on determination of the temperature dynamics inside the drying formulation. Extra lyophilisation runs were made in order to get additional drying kinetics information in the form of mass change at different time intervals. The aim of

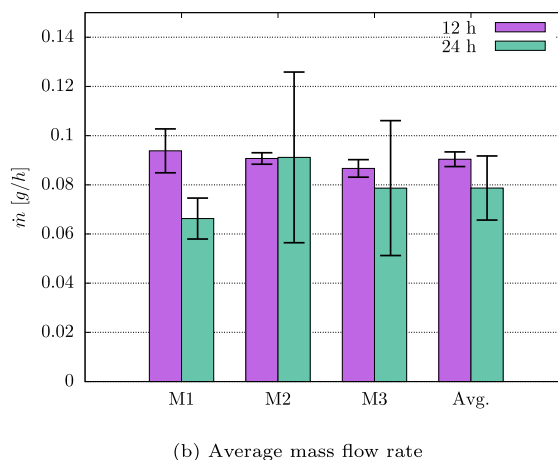
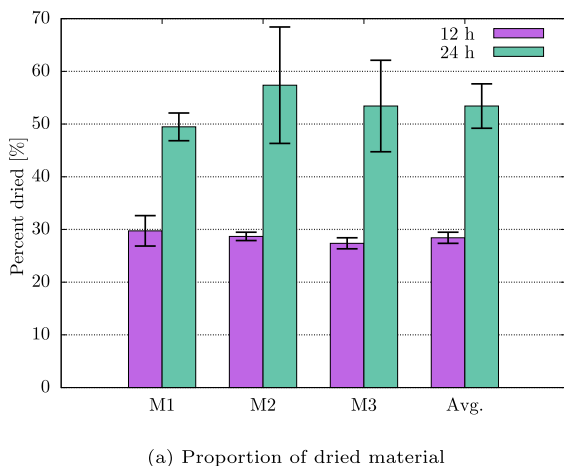


Fig. 3. Results of mass measurements after 12 and 24 h of primary drying. Results are shown for the three experimental runs as well as their average.

the additional runs was to determine the change of vial mass, and to calculate average mass flow rates. The additional runs were carried out without the insertion of the thermocouples and holders, making comparison with the results of the numerical model more realistic. The implemented protocol was the same as discussed in the Section 2.3, with the exception that the experiment was stopped after 12 h or 24 h of primary drying. After the runs were stopped, the vials were weighed using the Kern KB 650-2 N scale with ± 0.01 g accuracy. The purpose of this was to obtain the sublimed mass after 12 h and after 24 h of primary drying. For every interval 3 runs were performed, and their results averaged. Due to the fact that the freezing phase was not controlled, the mass of the centre vial (the vial in position 19) and vials in the first row around it (vials in positions 12, 13, 18, 20, 25 and 26), were also averaged to yield the final result. Based on this procedure the confidence interval for the obtained mean values was calculated, using the Student's t distribution. Results are presented in Fig. 3.

3. Deterministic numerical model for computation of lyophilisation in a vial

The process of sublimation starts when a positive pressure difference is established between the vapour pressure at the sublimation surface and partial pressure of the vapour in the surrounding gas phase. The mass flow rate can be calculated as

$$\dot{m} = dm/dt = A_p(p_v^* - p_o)/R_p, \tag{1}$$

with the A_p the inner cross-sectional area of the vial and R_p the resistance to the mass transfer. In order to have a unique definition of the R_p , the water vapour pressure at the sublimation front is set equal to the water vapour saturation pressure at the temperature of the interface:

$$p_v^* = 133.32Pa \cdot \exp\left(23.9936 - \frac{2.19\Delta H_v}{T}\right) \tag{2}$$

while the p_o is set as the system pressure in the drying chamber. With known value of the mass flow rate, which can be obtained gravimetrically from an experiment, or which is instantly available at the end of each time step computation in the case of using a dedicated vial lyophilisation model [26], the R_p value can be evaluated as

$$R_p = A_p(p_v^* - p_o)/\dot{m} \tag{3}$$

The sublimation of the frozen solvent presents a heat sink, acting on the frozen solvent, which would lead to undercooling of the sublimation front, and would eventually stop the mass transfer if no heat would be supplied to the vial. Therefore, in order to balance the sublimation, enthalpy heat is supplied, predominantly through the heating of the

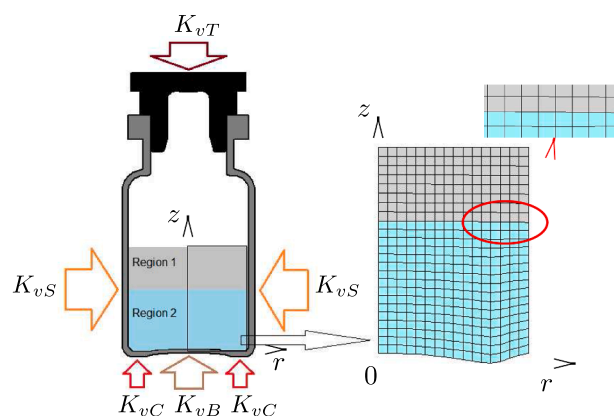


Fig. 4. Interior of the vial with stopper (left) - cake as Region 1, frozen solution as Region 2, heat input contributions, implemented computational grid (magnified, right). The following heat sources are presented: K_{vC} is the heat conduction from the shelf to the vial, K_{vB} is the heat radiation and convection from the bottom shelf, K_{vS} and K_{vT} are the contributions coming from the surrounding rarefied gas on the sides and the stopper at the top. Axisymmetric numerical model supports curved sublimation front, as is shown in the zoomed part of the grid.

shelves in the lyophiliser. In the case of laboratory type devices, the heat also comes from the chamber walls, especially for vials at the corners and edges of the shelf. The overall supplied heat flux \dot{Q} can, in general, be expressed as proportional to the heat transfer coefficient K_v , cross-sectional area of the vial A_v and temperature difference between the exterior T_{sh} and the interior of the vial T_v , as

$$dQ/dt = K_{vE}A_v(T_{sh} - T_v) \tag{4}$$

It has to be noted that the K_{vE} is an equivalent heat transfer coefficient, where contributions from heat conduction and heat radiation are included, without the need to take into account the heat convection, a consequence of a very low system pressure. In Fig. 4, heat inputs in the form of specific K_v 's corresponding to specific vial surface regions, are denoted. At the part of the vial in direct contact with the shelf area, the K_{vC} is considered equal to

$$K_{vC} = K_{vC,exp} \frac{A_v}{A_{contact}} \tag{5}$$

with the coefficient $K_{vC,exp}$ related to the whole cross-sectional area of the vial. As the implemented axisymmetric numerical model of lyophi-

lyophilisation does take into account that only a part of the vial bottom is in direct contact with the shelf, a scaled value of $K_{vC,exp}$, Eq. (5), has to be applied in the numerical evaluation. In our case, the $A_{contact}$ was determined experimentally to be 15.7% of the vial bottom area [10]. In the gap between the plate and the vial bottom heat conduction through the gas, as well as heat radiation between the two surfaces, are present, contributing to the overall K_{vB} value. With a corresponding heat conduction model form of [1] and the heat radiation contribution cast in a form appropriate for the temperature difference at the bottom $T_{sh} - T_v$, the K_{vB} is

$$K_{vB} = \sigma_B F_{12,b} \left(T_{sh} + T_v \right) \left(T_{sh}^2 + T_v^2 \right) + \frac{C_2 p_{syst}}{1 + \frac{l_b}{\lambda_{amb}} C_2 p_{syst}} \quad (6)$$

with σ_B the Boltzmann constant, T_{vB} the temperature of the vial at the bottom, p_{syst} the system pressure, λ_{amb} the water vapour free molecular heat conductivity, and l_b the integral conduction length at the bottom. The parameter C_2 takes into account the free molecular flow heat transfer coefficient Λ_o ,

$$C_2 = \Lambda_o \left(\frac{\alpha_C}{2 - \alpha_C} \right) \left[\frac{273.15}{T_{gas}} \right]^{0.5} \quad (7)$$

and the temperature of the gas, approximated as equal to the shelf temperature. The α_C is the surface accommodation parameter, its value dependent on the technical system, specifically the shelf and vial surface properties used for lyophilisation. As the uncertainty analysis is focused on the central vial positions, the heat radiation from the side was neglected, leaving the heat to contribute only through conduction through the gas,

$$K_{vS} = \frac{C_2 p_{syst}}{1 + \frac{l_s}{\lambda_{amb}} C_2 p_{syst}} \quad (8)$$

with l_s the integral conduction length at the side. Since the test vials were positioned in the middle shelf, the heat input at the top of the vial was composed of heat radiation from the top shelf, as well as heat conduction through the gas,

$$K_{vT} = \sigma_B F_{12,t} \left(T_{sh} + T_v \right) \left(T_{sh}^2 + T_{vT}^2 \right) + \frac{C_2 p_{syst}}{1 + \frac{l_t}{\lambda_{amb}} C_2 p_{syst}} \quad (9)$$

with T_{vT} being the vial stopper surface temperature and l_t the integral conduction length at the top. Inside the vial, the supplied heat from the shelves is consumed predominantly by the phase change process, as well as by the increase of the formulation temperature, which is covered by the heat and mass transfer within the frozen, as well as the already dried, porous part (cake) of the product. The heat from the surroundings, which is transferred to and conducted through the vial walls, is then in Region 1, Fig. 4, transferred by conduction and convection, due to vapour and inert gas convective fluxes, with additional heat sink due to the desorption of water from the porous part of the drying substance. In Region 2, the heat transfer mechanism is the heat conduction, governed only by the frozen solution thermal conductivity λ . At the sublimation front, where the frozen and porous parts of the domain are in contact, the frozen solvent undergoes a phase change, consuming the sublimation enthalpy for this process. In the vial lyophilisation model the conservation of mass needs to be computed only in Region 1, for both water vapour and inert gas, which are both treated as ideal gases. The critical part for the performance of the lyophilisation model is the correct modelling of water vapour and inert gas mass fluxes, where the dusty gas model is applied [27]. It builds on a combination of Fick's diffusivities, as well as the effect of the Knudsen diffusivity,

Table 1
Values of model parameters.

Variable	Value
A_p	$314.2 \cdot 10^{-6} \text{ m}^2$
A_v	$380.1 \cdot 10^{-6} \text{ m}^2$
$A_{contact}$	$59.6 \cdot 10^{-6} \text{ m}^2$
C_1	$8 \cdot 10^{-6} \text{ m}$
$F_{12,b}$	0.17
$F_{12,t}$	0.12
$K_{vC,exp}$	$3.67 \text{ W}/(\text{m}^2\text{K})$
l_b	$0.5 \cdot 10^{-3} \text{ m}$
l_s	$3.5 \cdot 10^{-3} \text{ m}$
l_t	$47.0 \cdot 10^{-3} \text{ m}$
M	18 kg/kmol
$p_{syst} = p_o$	6.67 Pa
R	8314 J/(kmol K)
T_{sh}	$-18 \text{ }^\circ\text{C}$
T_{vT}	$-18 \text{ }^\circ\text{C}$
α_C	$0.40 \text{ kg}/\text{m}^3$
ΔH_v	$2840.2 \cdot 10^3 \text{ J}/\text{kg}$
Λ_o	$1.99 \text{ W}/(\text{m}^2 \text{ KPa})$
λ_{amb}	$0.025 \text{ W}/(\text{mK})$
σ_B	$5.67 \cdot 10^{-8} \text{ W}/(\text{m}^2\text{K}^4)$

$$K_{kn} = \frac{\lambda_p}{3} \sqrt{\frac{8RT}{\pi M}} \quad (10)$$

with the latter playing the most important role in the case of the low system pressure values needed in lyophilisation. With λ_p the molecular free path in the order of a typical pore diameter of the dried cake, ϵ its porosity and τ its tortuosity, the effective Knudsen diffusivity can be defined as

$$K_{kn,eff} = \frac{\epsilon}{\tau} \frac{d_p}{3} \sqrt{\frac{8RT}{\pi M}} \quad (11)$$

As it is seldom possible to measure the pore size and tortuosity exactly, the following form of the effective Knudsen diffusivity is used:

$$K_{kn,eff} = C_1 \sqrt{\frac{RT}{M}} \quad (12)$$

with the model parameter C_1 as

$$C_1 = \frac{\epsilon}{3\tau} \sqrt{\frac{8}{\pi}} d_p \quad (13)$$

The model for the mass transfer from the porous cake, that was implemented to include the effects of the secondary drying when all the ice has been sublimed, is based on the first order chemical kinetics, and is reported in [23]. It has proven as adequately accurate to be included in the present analysis, although, in the case when the secondary drying step would also be included in the sensitivity analysis, this would require an additional detailed study of equilibrium conditions and determination of mass transfer kinetic parameters.

As the goal of the paper is the uncertainty analysis of the primary drying step, extensive descriptions of the physical models in the form of the mass and energy conservation equations for both regions inside the vial that form the basis for the implemented BEM based numerical model for both the primary and the secondary drying steps, are omitted here, but are given in [23,26]. The material properties and values of model parameters reported in this paper are summarised in Table 1. The material properties for the 5% mannitol-water solution used for the computational model of heat and mass transfer inside the vial, are

reported in [23].

4. Numerical simulation of the lyophilisation process in the vial

To assess the relative importance of parameters in the lyophilisation process, we coupled the deterministic simulation of the process with the Stochastic Collocation Method. The details of the deterministic mathematical model, as well as its numerical implementation, which was used for computing the temperature distribution inside the frozen, as well as porous parts, and for computing the mass flow rates of sublimation, are given in [26], together with a mesh sensitivity analysis. The implemented numerical model is based on the Subdomain form of the Boundary Element Method (BEM), which is a type of Weighted Residuals Method, applied to the resulting set of heat and mass conservation equations in the form of partial differential equations. The numerical solution is based on the axisymmetric representation of the vial. This allows taking into account the curved shape of the sublimation front, which occurs due to different heat transfer conditions at the bottom and sides of the vial. Recent studies have shown [28] that the shape of the front can be more complex, featuring fragmented or fractal structure, while, at the same time, sublimation fingering can occur. These effects can be a source of uncertainty, but are not modelled with our approach. The numerical solution algorithm uses discretisation of the computational domain into boundary and domain elements, see Fig. 4, and implementation of the Finite Difference (FD) second order asymmetric numerical time marching scheme. The computational domain consisted of 19 times 16 internal domains, and the time step was varied dynamically between 0.1 s (the heat up period) and 1 s for the primary phase. The deterministic simulation requires known boundary conditions for the heat transfer to the vial, given in the form of K_v 's (Fig. 4), with the implementation of the models for calculation of the K_v 's reported in [10].

4.1. Selection of the parameters for the sensitivity analysis

As is evident from the previous Section, the computation of the lyophilisation by using a deterministic lyophilisation model requires the specification of several model parameters and assumptions. Determination of these parameters could not always be achieved by performing dedicated experiments, or implementing high-end experimental techniques. The most obvious example is determination of the C_1 value, which relates to the internal geometrical structure of the dried cake, which is different in the vicinity of the cake surface, vial walls, or in the bulk of the cake, a result of spatially varying heat transfer rate conditions in the freezing part of the lyophilisation. As the implemented values of the model parameters influence the computational outcome of the deterministic model directly, a sensitivity analysis of these parameters needs to be done. Since the computational requirements of the stochastic analysis are related directly to the number of influence parameters, a sensitivity analysis is needed with a limited number of the most important parameters. The mass transfer resistance in the porous cake presents the first significant influence on the computational results. The internal structure of the porous cake can be described as an open pore channel system, where the interaction of the sublimed vapour molecules and porous walls contribute significantly to the hydraulic resistance of the cake, which, in turn, increases the pressure drop within the cake. The in-cake pressure drop leads to a decrease in the effective pressure difference between the sublimation front and the surroundings of the cake, which drives the sublimation process. The main model parameter connected with the internal cake geometry is, therefore, the C_1 , which is obvious, as it is defined with respect to the value of the typical pore diameter. The determination of a representative pore diameter value is possible by using dedicated experimental techniques, like a SEM analysis [29] or X-ray μ -Computed Tomography measurements [30]. However, the value of the C_1 from such an analysis should only be viewed as an estimation and not an exact value, [31,23],

Table 2

Selected model parameters with selected lower and upper bounds of parameter values. The C_1 governs the gas diffusivity in the dried cake, α_c is the surface accommodation parameter appearing in the heat conduction model, p_{sys} is the system pressure, K_{vC} is the heat transfer coefficient between the shelf and the vial and λ is the thermal conductivity of the frozen solution.

Parameter	Unit	Lower bound	Upper bound
C_1	μm	6	10
α_c	–	0.35	0.45
p_{sys}	Pa	6.2	7.2
K_{vC}	$\text{W}/(\text{m}^2\text{K})$	2.67	4.67
λ	$\text{W}/(\text{mK})$	2.161	3.161

therefore, it is selected as the first uncertainty parameter. On the side of the frozen part of the formulation, the thermal conductivity of the frozen solution λ , which controls the conductive heat transfer from the heated glass walls to the sublimation front, is the most important parameter. Since the frozen formulation is a mixture of the solid matrix, which, typically, consists of several active and passive components and the frozen solvent, the effective thermal conductivity is a function of the mixture composition. When the mixing rule is used as a means to calculate the effective conductivity, the result depends on the correct data on the species fractions, and on the correct data on the thermal conductivity of pure substances, which are rarely documented by the manufacturers or in the open literature. To take this effect into account, the thermal conductivity of the frozen part of the solution λ , was chosen as the second sensitive parameter. On the part of the heat transfer to the vial, the system pressure and accommodation coefficient α_c are the next two vital parameters for inclusion into the set of sensitive parameters. The choice of system pressure is related to the fact that the heat conduction through the rarefied gas, Eq. (8), which acts on all the surfaces that are not in direct contact with the shelf, is related directly to the value of the system pressure. As the system pressure is maintained by the operation of a vacuum pump, and also depends on the obtained value from the type of pressure sensor and its position in the drying chamber, the real value of the system pressure may differ from the value predefined in the lyophilisation protocol. The importance of the system pressure for the freeze-dryer design was exposed by Barresi et al. [32,33]. On the other hand, the value of the accommodation coefficient α_c depends on the materials of the shelf and vial surfaces, and can rarely be determined exactly [34]. As the heat conduction from the gas contributes an important part of the overall supplied heat, both parameters, the α_c , as well as the system pressure p_{sys} , were selected for the sensitivity analysis. The last model parameter chosen was the K_{vC} , the heat transfer coefficient of the direct contact of the vial with the shelf surface, which also depends on the surface properties of the shelf and the vial [34]. We considered all five parameters as random variables distributed uniformly between the upper and lower bounds defined, given in Table 2. The selection of these parameter values was based on an extensive study of the scientific reports [35,34,36–38], as well as performed verification and validation cases [26,23,10]. The sensitivity analysis, presented in the following Sections, was focused exclusively on the primary drying phase, as this step is the critical step in the drying stage of lyophilisation, i.e. the freeze drying step. Among the main computational results, the computed temperature at selected heights, the percentage dried and the maximum temperature in the frozen material during the primary drying, were the focus of the investigation. The computed temperature at selected heights is readily available at each time instant, at the same positions as used for placing the thermocouples. The percentage dried was calculated based on the computed position of the sublimation front, which defined the volumes of the dry cake and the still frozen solution, with percentage dried defined as the ratio of the volume of the dry cake and the initial volume of the frozen material. The maximum temperature was defined based on scanning the

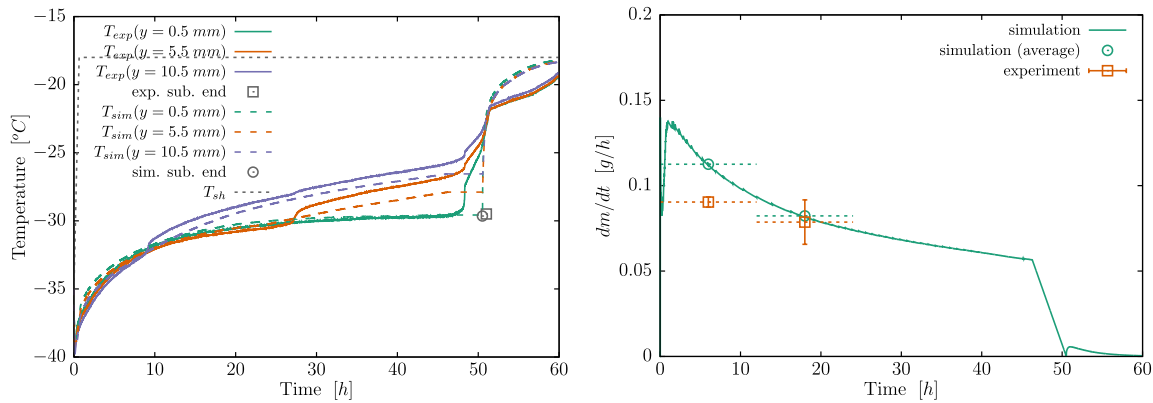


Fig. 5. Simulation results of the deterministic model with parameters from the middle of the used bounds in Table 2. Experimental and computed temperatures at selected thermocouple positions (left) and mass flux (right) are shown.

computational results at all evaluated grid points at each computed time instant as the maximum temperature within the still frozen part of the material.

4.2. The Stochastic Collocation Method

A description of the Stochastic Collocation Method, implemented for the uncertainty analysis, is given in the following. Let σ represent one of the input parameters. We consider all of the parameters to be random variables uniformly distributed in a range $\sigma \in (\sigma_{min}, \sigma_{max})$. Their probability distribution function (PDF) is

$$p(\sigma) = \begin{cases} \frac{1}{\sigma_{max} - \sigma_{min}} & \sigma \in (\sigma_{min}, \sigma_{max}) \\ 0 & \text{elsewhere} \end{cases} \quad (14)$$

Let the number of random variables be n . Additionally, let our deterministic model, which simulates the freeze drying process, be denoted by $y(\sigma_1, \dots, \sigma_n)$. In this case, statistics for our deterministic model, such as expected value μ_y , variance var_y , skewness $skew_y$ and kurtosis $kurt_y$, may be calculated using

$$Y_i = \int_{-\infty}^{\infty} \dots \int_{-\infty}^{\infty} [y(\sigma_1, \dots, \sigma_n)]^i p(\sigma_1) \dots p(\sigma_n) d\sigma_1 \dots d\sigma_n \quad (15)$$

$$\mu_y = Y_1, \quad var_y = Y_2 - \mu_y^2 \quad (16)$$

$$skew_y = \frac{Y_3 - 3\mu_y \cdot var_y - \mu_y^3}{var_y^{3/2}}, \quad kurt_y = \frac{Y_4 - 4\mu_y Y_3 + 6\mu_y^2 Y_2 - 3\mu_y^4}{var_y^2} \quad (17)$$

Due to the fact that the PDFs are non-zero only in a limited range, we can change the integration limits of (15) as

$$Y_i = \int_{\sigma_{min,1}}^{\sigma_{max,1}} \dots \int_{\sigma_{min,n}}^{\sigma_{max,n}} [y(\sigma_1, \dots, \sigma_n)]^i p(\sigma_1) \dots p(\sigma_n) d\sigma_1 \dots d\sigma_n. \quad (18)$$

Making use of the following change of variables $\xi^{(j)} = \sigma_{j,max} - \sigma_{j,min} \frac{\sigma_j + 1}{2}$ and considering the PDF definition (14) we obtain

$$Y_i = \frac{1}{2^n} \int_{-1}^1 \dots \int_{-1}^1 [y(\xi^{(1)}, \dots, \xi^{(n)})]^i d\xi^{(1)} \dots d\xi^{(n)} \quad (19)$$

The integral (19) can be calculated using Gauss–Legendre quadrature. Considering N Gauss–Legendre points, one finds

$$Y_i \approx \frac{1}{2^n} \sum_{j=1}^N \underbrace{\sum_{k=1}^N \dots \sum_{l=1}^N}_n [y(\xi_j^{(1)}, \xi_k^{(2)}, \dots, \xi_l^{(n)})]^i w_j w_k \dots w_l, \quad (20)$$

where $\xi_j^{(t)} = \sigma_{t,min} + (\sigma_{t,max} - \sigma_{t,min}) \frac{\eta_j + 1}{2}$ and η_j and w_j are Gauss–Legendre points and weights. The main drawback of this procedure is the fact that it requires N^n evaluations of the deterministic simulation model y . In this paper, we consider $n = 5$ parameters and three different quadrature strategies, having $N = 3, N = 4$ and $N = 5$ collocation points. In the case of $N = 3$, we could employ the Gauss–Legendre quadrature and perform $3^5 = 243$ simulations. The required computational effort for $N = 4, 5$ would be 4^5 and 5^5 simulations, which is too large. To avoid this bottleneck, we proposed to calculate the integral (19) using the Smolyak [39–41] sparse grid approach. Using Smolyak quadrature the integral is approximated by

$$Y_i \approx \frac{1}{2^n} \sum_{i=1}^{N_s} [y(\xi_i^{(1)}, \xi_i^{(2)}, \dots, \xi_i^{(n)})]^i w_i, \quad (21)$$

where $\xi_i^{(t)} = \sigma_{t,min} + (\sigma_{t,max} - \sigma_{t,min}) \frac{\eta_i + 1}{2}$ and η_i and w_i are sparse grid points and weights. The number of sparse grid points in (21) is much smaller than the number of points needed by the Gauss–Legendre approach (20), i.e. $N_s \ll N^n$. In order to calculate the points and weights for the sparse grid, we employed the Tasmanian library [42,43] using Clenshaw Curtis fully nested collocation points. Having fully nested points has an additional benefit of reusing $N = 3$ simulations as a part of $N = 4$ simulations, and reusing $N = 4$ simulations for the $N = 5$ data set. Statistical quantities, such as variance, for example, may be calculated via (15) when all n parameters are varied. Such an approach is called a Full Tensor Product (FTP) approach. Alternatively, when only one of the parameters is varied, we have the One-At-a-Time (OAT) approach. Statistical quantities may be compared between the OAT and the FTP approaches. In this way, we can study how the uncertainty of the output of the model y can be apportioned to different sources of uncertainty [44]. We define the sensitivity index of each random variable as

$$S_i(y) = \frac{var_{y,OAT(i)}}{var_y}, \quad (22)$$

where $var_{y,OAT(i)}$ is the variance obtained using the OAT approach, with i denoting the parameter, which was assumed to be a random variable. The var_y is the variance obtained using the FTP approach (15). Large values of the sensitivity index indicate bigger relative importance of the random variable.

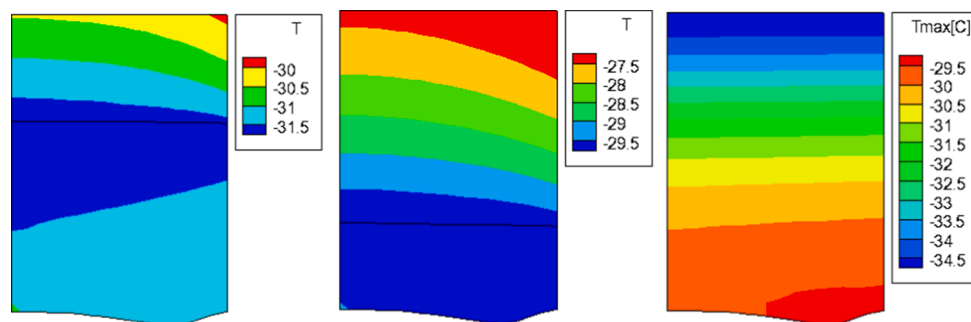


Fig. 6. Computational results of the BEM based deterministic model using values of target parameters from the middle of the used bounds in Table 2: Computed temperature field after 12 h (left) and after 30 h (middle); maximum reached temperatures in the frozen zone during the primary phase (right). The shelf temperature was set to $T_{sh} = -18$ °C and is kept konstant during the primary phase.

5. Results

Based on the selected parameters C_1, α_C , the system pressure p_{syst} , K_{VC} and the thermal conductivity of the frozen material λ , defined in Section 4.1, deterministic numerical simulations can be carried out. In the following, a sample deterministic simulation for a single set of the selected parameter values is presented and analyzed first, followed by the results of implementation of the Stochastic Collocation Method (SCM) used to evaluate the expected values, variance, Standard Deviation, skewness and kurtosis for several variables given by the deterministic solver: The primary drying time and time traces of the temperature at various positions along the height of the vial, the vapour mass flow calculated at the top of the material, the fraction of the dried material and the maximum temperature in the material.

5.1. A sample deterministic simulation

Let us first look at the results of a typical deterministic simulation, with the following choice of parameters: $C_1 = 8 \mu\text{m}$, $\alpha_C = 0.4$, $p_{syst} = 6.7 \text{ Pa}$, $K_{VC} = 3.67 \text{ W/m}^2\text{K}$, $\lambda = 2.661 \text{ W/mK}$. As is evident from Fig. 5, the agreement between the experimental temperature time series and the computationally obtained temperature values at the same positions is very good, especially as long as there is a frozen phase present in the domain, i.e. during the primary drying phase. A well defined lyophilisation protocol can be observed, with almost a constant temperature at the bottom of the vial, and an increase in temperature readings once the sublimation front has passed a thermocouple position. The transition from the characteristic dynamics of the primary drying phase to the characteristics of the secondary drying phase, which appears in the form of a fast cake temperature increase up to the predefined shelf temperature, is well defined in the case of the computational model. This is the point when all the frozen solution is sublimed, and, as the heat input is no longer consumed predominantly for the phase change, a steep increase in temperature is the consequence. In the experimental case, the exact definition is not trivial [45]. Here, the definition based on the time instant when the available temperature readings at three distinct heights seemingly merge into a single reading, see Fig. 5 left, is adopted as the end of the primary drying. If the lyophiliser is equipped with both the Pirani and capacitance pressure sensors, the drop in Pirani sensor readings could also be used for determination of the end point. A temperature overshoot at the end of the primary drying protocol is mainly a result of the external influences, which are frequently noticeable in the case of a laboratory type lyophilisation device [23], but can, in the case of using the Pirani sensor for the control of the system pressure, also be connected to the rise of the system pressure and increased heat transfer rate. In the right panel of Fig. 5 the simulated mass flow rate is shown, and compared to two experimental measurements at 12 and 24 h after the start of primary drying. It is evident that the overall agreement is very good, with the exception of the mass flux comparison after 12 h,

which is to be attributed to a higher experimental uncertainty of the gravimetric mass determination, and a faster numerically computed initial heat-up part of the process. The latter could be a consequence of the characteristics of the transition from the freezing stage to the sublimation stage, where the temporal dynamics of the decreasing of the system pressure dominate the sublimation phenomena, and in order to have a better agreement in this stage, a dedicated numerical transition model should be developed in the future. In Fig. 6 right, the computational results of the temperature field inside the drying material at two different time instants are shown, together with a plot of the maximum reached temperatures in the frozen phase during the primary drying. The temperature plot after 12 h shows that the heating up part of the primary phase is not yet overcome, as the bottom part of the frozen region is at a noticeably higher temperature than the interior. As the primary drying phase reaches its equilibrium phase after around 20 h, the temperature inside the frozen phase has a much lower temperature gradient (see the plot in the middle of Fig. 6), and also does not change noticeably with respect to time, until the last part of the primary phase. The higher temperature levels in the upper part of the material are attributed to the heating up of the porous cake, where the heat sink due to water desorption is lower than the supplied heat from the top and sides of the vial, leading to the increase of the cake temperature. From the maximum temperature plot in the frozen phase (Fig. 6, right) it can be observed that the maximum reached temperatures are near the bottom and in the direct vicinity of the vial's contact with the shelf, which presents the critical area in the primary drying phase, and which are, in the present case, reached in the last part of the primary drying phase. The vial's central position on the shelf surrounded by other vials effectively limits heat transfer from the side, and since the applied computational model does not resolve lateral heat conduction in the glass wall directly, the effect of which could contribute to a more pronounced curvature of the sublimation surface, the computational results show only a minor effect of the curving of the sublimation surface, see Fig. 4.

5.2. Stochastic Collocation Method results

In the case of the uncertainty analysis, two groups of analyses were carried out. The One-At-a-Time (AOT) analysis, in which only a single parameter was varied, was evaluated using 9 collocation points ($n = 1$, $N = 9$). Then the full tensor approach with all five parameters and 3, 4 and 5 collocation points ($n = 5, N = 3, 4, 5$) was calculated via the sparse Smolyak quadrature. A total of 241 simulations were performed for the case $N = 3$, 801 for the case $N = 4$ and 2433 for $N = 5$. The reason for running simulations with a different number of collocation points was to prove the convergence of the statistical quantities.

5.2.1. SCM: One At a Time results

We chose $N = 9$ collocation points and varied each of the parameters separately, so that we used $n = 1$ and performed 9 deterministic simu-

Table 3

Uncertainty of the determination of primary phase drying time obtained via OAT analysis. Clearly, C_1 and K_{vc} are the most influential parameters, while the system pressure p_{syst} and thermal conductivity λ have an almost negligible effect.

OAT parameter	Primary drying time [h]
C_1	50.8 ± 2.4
α_c	50.5 ± 1.1
p_{syst}	50.2 ± 0.2
K_{vc}	50.6 ± 1.8
λ	50.5 ± 0.06

lations for each of the parameters. The expected value of the primary drying time and the Standard Deviations based on the OAT analysis of each of the five parameters are presented in Table 3. The end of the primary phase was defined as the time when all the frozen solvent has been sublimed, i.e. only the porous cake remains in the vial. The greatest uncertainty was found with respect to the change in values of the C_1 and K_{vc} , followed closely by the α_c . On the other hand, the system pressure p_{syst} and the thermal conductivity of the frozen formulation λ have very little influence on the primary drying time. In the Figs. 7 and 8 we present the results of the OAT study - the expected values of the observed variables and their Standard Deviations. Where possible, the comparison is given with the experimentally measured values. The temperature-time traces (Fig. 7) show good agreement with the experimental measurements. The Standard Deviation of the temperature is the largest after the sublimation front has moved past a sensor at a certain height and the physical properties are altered due to change to the porous cake. During this period the most influential parameters are C_1 , α_c and K_{vc} . In contrast, the expected values of the frozen solution temperature during the primary phase are less affected by the changes in the parameters, although deviations in the order of a few degrees can still be expected, especially at the bottom of the frozen material. This position presents the critical position during the primary drying, as this is also the area of the largest heat input into the vial, so even a few K difference can be important. When studying the time trace of the mass flow rate (Fig. 8), we again observe the greatest uncertainty at the end of the primary drying process, when all the ice has sublimed and the desorption and diffusion take place of water vapor through the porous material. Comparing the obtained computational results with the two measured flow rates (see Section 2.5), the results for the second (24 h) gravimetrically measured mass flow rate show excellent agreement. Although the agreement with the averaged values of the first measurement (12 h) is only moderate, also taking into account the maximum measured values (see Fig. 5) and the nature of the used gravimetric method, the computational results can still be considered as good. The percentage of the dried material graph, linked directly to the dynamics of the movement of the sublimation front, seems to be stable, and largely unaffected by the changes in the input parameters. In contrast, the maximum temperature (Fig. 8) exhibits the largest Standard Deviation of approximately 1K in the case of the C_1 parameter, and even less in the case of other parameters, meaning that the maximum temperatures of the frozen solution are less affected by the uncertainties in the heat transfer parameters, and are mainly a result of the general setting of the system pressure and shelf temperature.

5.2.2. SCM: Full tensor product results

A full tensor product stochastic analysis was performed taking all five input parameters into account. The number of collocation points ($N = 3, 4, 5$) was varied, in order to prove that the results converge, and that the choice of the number of collocation points is appropriate. The results of the convergence study are presented in Table 4, where we can observe that changing the number of collocation points does not influence the results strongly. In the Fig. 9 the time traces of the expected values and

Standard Deviations of several quantities are shown. The mass flow rate shows the largest Standard Deviation in the period that begins after all the frozen ice was sublimed. When desorption is the main source of water vapour release and the properties of the porous dried material are important, we observe the greatest uncertainty in the water vapour mass flow rate leaving the material. The percentage of the dried material increases approximately linearly with time, and is influenced to a lesser extent by the changes in input parameters. The Standard Deviation reaches a few percent in the secondary drying stage. The maximum temperature in the material has the Standard Deviation of 2 °C, which is an important design consideration, since in most applications a collapse can occur when a critical temperature is reached in the material. The maximum temperature deviation reaches its nearly highest value already at the end of the heating up part of the primary phase, which, when combined with local temperature distribution in the frozen phase, shown in Fig. 6 (the left panel, after 12 h), presents an important limitation in the process protocol development, as a too rapid temperature increase could easily lead to exceeding the maximum allowed temperature level in the material and local transition to a liquid phase. On the other hand, the temperature at different heights in the material has a small uncertainty during the primary drying stage, when ice is still present, and increases significantly after the point at which the ice at a certain height has sublimed.

Time traces of skewness and kurtosis are shown in Fig. 10. Looking at kurtosis, we observe that, during the primary drying, the distribution of all variables is platykurtic (i.e. has kurtosis less than 3). This means that the distribution is wide and has thinner tails, so that few simulation results are at the outer edges of the parameter space. Compared to normal distribution, which has a kurtosis of 3, our simulation results are focused more strongly around the centre of the parameter space. Apart from the very start of the simulations, the distribution of the results does not seem to be significantly skewed, since, for most variables, the skewness is very close to zero. This means that the simulation results are distributed evenly around the expected values.

5.3. Sensitivity index results

The sensitivity index, Eq. (22), is defined as the ratio of the Standard Deviation obtained by the OAT approach and by the full tensor product approach. It is a measure of the relative importance of the individual parameters. Fig. 11 shows the temporal evaluation of the sensitivity index for the temperature at different heights above the bottom of the vial. We observed a significant change in the sensitivity index when the sublimation front reached the temperature probe. While a location is still frozen the C_1 parameter is the most important. After the sublimation front reaches a probe position, the importance of the C_1 parameter decreases significantly. In the lyophilisation model, the C_1 parameter describes the Knudsen type vapour diffusion through the porous cake, which is a result of the phase change process at the sublimation front. The supplied heat for the process is consumed mainly as a sublimation enthalpy, therefore, the change in the mass transfer resistance of the cake, i.e. the C_1 value, influences the sublimation rate directly and, hence, the temperature in the frozen material. At the same time, the sensitivity indices of K_{vc} and α_c increase, which means that these parameters play a more important role in the secondary stage of the drying, when water is desorbed from the remaining solid porous material. It must be noted that the applied lyophilisation computational model [26] takes the secondary drying effects into account already during the primary drying stage, as soon as the porous cake is formed. Of course, the effects of the secondary drying become more pronounced as the shelf temperature is increased during by the protocol defined secondary drying stage. As the mass transfer in the secondary stage is significantly less intensive than when sublimation takes place, the supplied heat through the direct contact and the gas conduction, with the corresponding parameters K_{vc} and α_c , has a more pronounced effect on the temperature in the porous cake. On the other hand, the sensitivity index

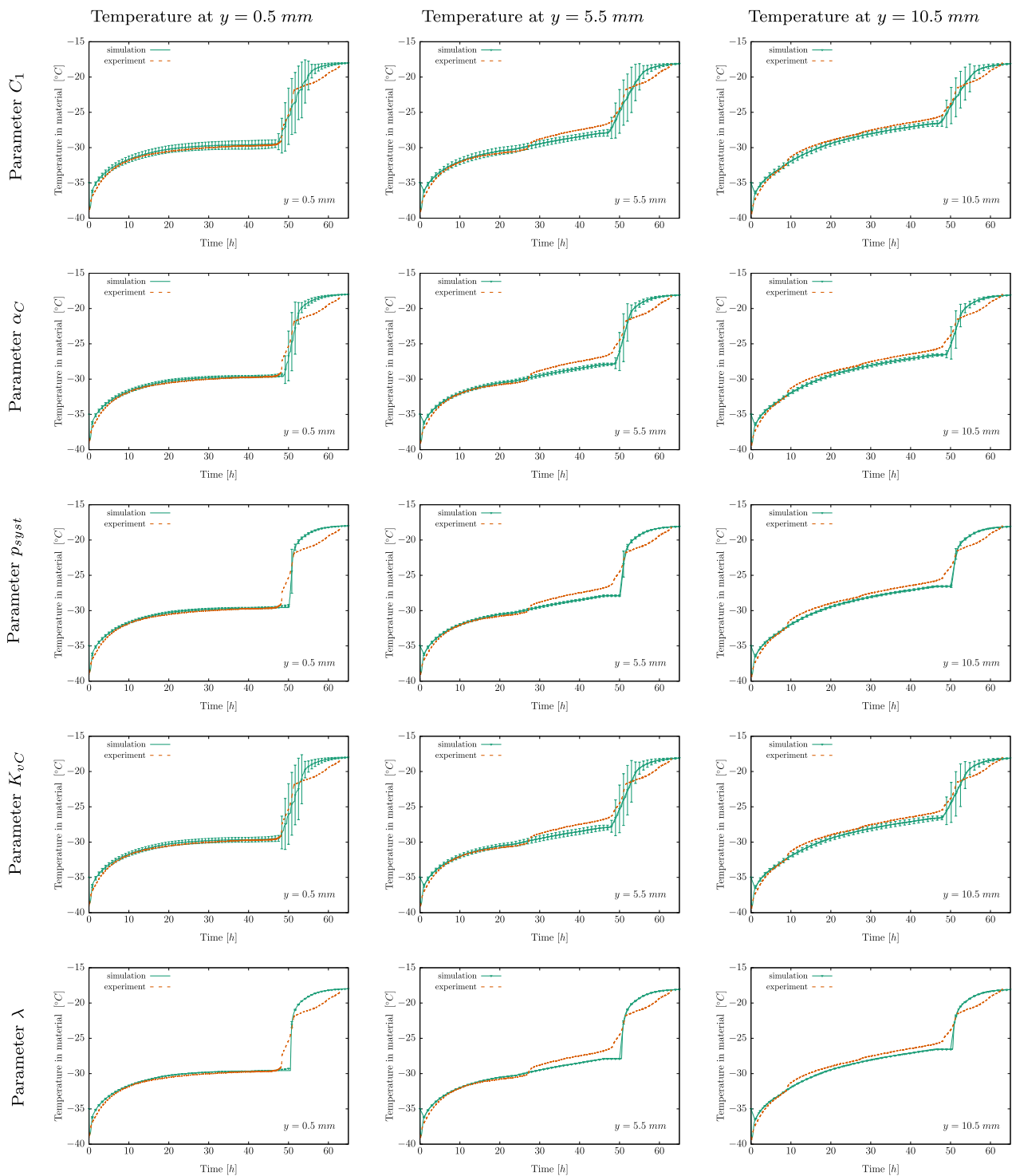


Fig. 7. Comparison of simulated and measured temperature at $y = 0.5$ mm (left), $y = 5.5$ mm (center) and $y = 10.5$ mm (right). Standard deviation obtained by OAT analysis for all parameters is shown: C_1 (top), α_C (second row), p_{syst} (third row), K_{vC} (fourth row) and λ (bottom).

of the system pressure p_{syst} is low, and this parameter does not play an important role in the drying dynamics, as long as a constant pressure drying regime is specified. There are also two ranges of strong oscillations in the sensitivity indices with respect to the C_1, K_{vC}, α_C , and to some extent also to the p_{syst} , as shown in Fig. 11. The first after about 44 h when the mass flow rate begins to decrease, and the second after about 50 h when the primary drying ends. Thereafter, the sensitivity indices decrease significantly when the primary phase ends and all ice has sublimed. The change in the sensitivity indices could, therefore, be used

as another means of the definition of the end of the primary drying phase. When only the secondary drying effects remain, i.e. when water desorption and transport through the porous cake are the only drying mechanisms, the sensitivity of C_1, K_{vC}, λ and α_C is comparable, while the sensitivity index of system pressure p_{syst} remains lower. Finally, Fig. 11 also shows the sensitivity indices for the maximum temperature in the material. We observe that the parameter C_1 has the greatest influence on the maximum temperature throughout the freeze drying process, followed by $K_{vC}, \alpha_C, \lambda$, and p_{syst} . As the C_1 is a material dependent value,

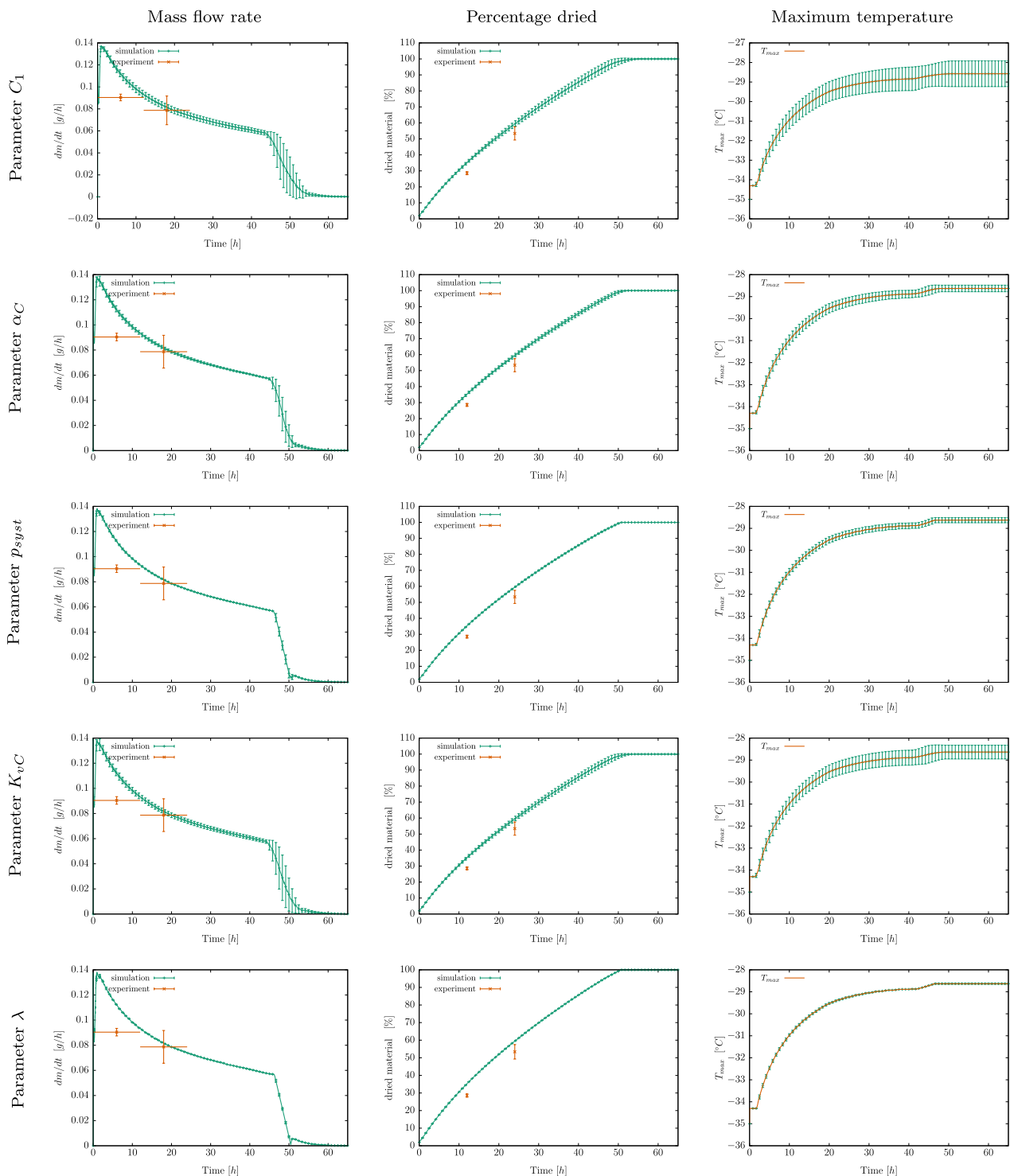


Fig. 8. Comparison of mass flow rate (left), share of dried material (center), maximum temperature (right) OAT analysis for all parameters: C_1 (top), α_C (second row), p_{sys} (third row), K_{vC} (fourth row) and λ (bottom).

special attention must be paid to the determination of this value when a new material is studied. The sensitivity index for the mass flow and the dried material fraction is given in Fig. 12. The mass flow diagram shows that, at the start of the primary drying stage, the most important parameters are K_{vC} and α_C , but after about 10 h of primary drying the C_1 parameter starts to dominate. This is a direct consequence of the heating up part of the primary drying, when the temperature at the sublimation front starts to increase from the freezing levels to the primary drying final level. At low temperatures the saturation pressure is low, leading to

a moderate increase in the mass transfer rate, see Eq. (1), and a large part of the supplied heat is transformed into a sensible heat. The sensitivity indices for the dried fraction of the material are approximately the same for C_1 , K_{vC} and α_C and negligible for the thermal diffusivity of the frozen material λ and the system pressure p_{sys} .

6. Conclusions

The coupling of the Stochastic Collocation Method with a deter-

Table 4

Uncertainty of the determination of primary phase drying time and temperature after 10 h of drying obtained via full tensor product analysis. As the number of collocation points N is increased, we see good convergence of results proving that result obtained with $N = 5$ are numerically converged.

N	Primary drying time [h]	Temperature after 10 h of drying		
		$T(y = 0.5 \text{ mm})$ [°C]	$T(y = 5.5 \text{ mm})$ [°C]	$T(y = 10.5 \text{ mm})$ [°C]
3	50.97 ± 3.24	-31.68 ± 0.61	-31.97 ± 0.61	-31.94 ± 0.60
4	50.99 ± 3.23	-31.67 ± 0.60	-31.96 ± 0.60	-31.93 ± 0.59
5	50.99 ± 3.24	-31.67 ± 0.61	-31.96 ± 0.61	-31.92 ± 0.60

ministic computational simulation of the lyophilisation allows the investigation of the susceptibility of the drying process to uncertainties in the input parameters. This information is crucial in the design phase of the lyophilisation process, in order to optimise energy consumption and drying time, and to ensure good product quality. The sensitivity analysis shows that, during the heating part of the primary drying stage, the heat transfer mechanisms from the shelf to the vial play the most important role, whereas, in the main part of the primary drying process, i.e. in the stationary temperature regime, this role is assigned to the mass transfer resistance of the porous cake. The maximum temperature sensitivity analysis shows that the design of the temperature ramp must

avoid a too rapid heating up, that could lead to melting of the frozen solvent, as this sensitivity is comparable to the maximum temperature sensitivity at the end of the primary drying phase. The sensitivity analysis showed that the most important heat transfer model parameters are K_{VC} and α_C , which are both linked to the geometrical and material properties of the vial, whereas the heat transfer rate can be controlled directly by a suitable level of the system pressure, where a capacitance sensor is preferred over the Pirani sensor, and the shelf temperature, the mass transfer resistance is affected mainly by the frozen solid structure established during the solid–liquid phase change phenomena in the freezing step. The Knudsen diffusivity based model parameter C_1 proves

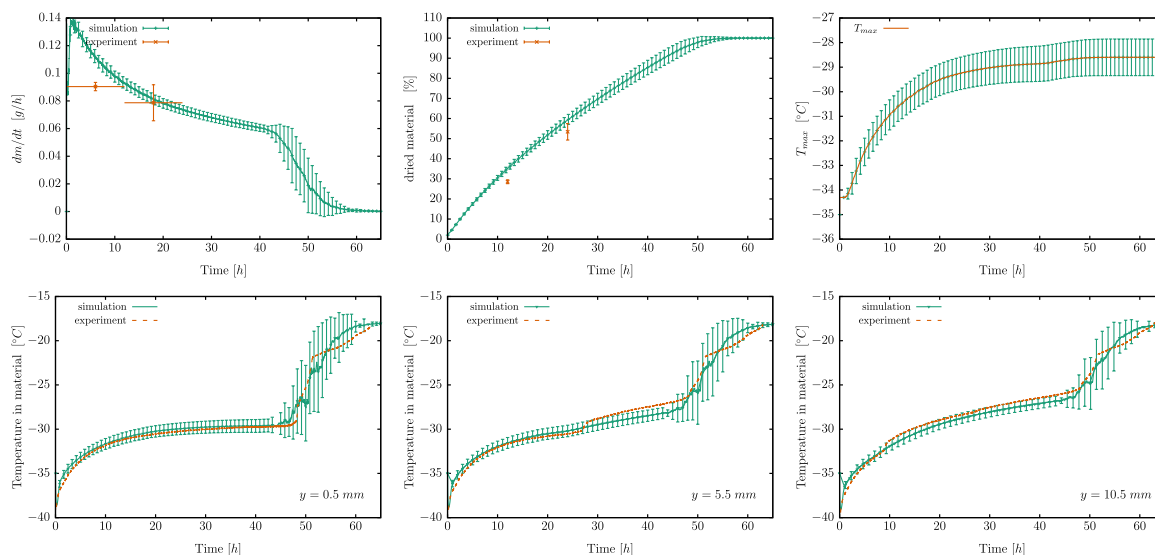


Fig. 9. Full tensor product stochastic collocation method results. Expected value and standard deviation are shown for the mass flux, dried share of material, maximum temperature and temperatures at $y = 0.5 \text{ mm}$, $y = 5.5 \text{ mm}$ and $y = 10.5 \text{ mm}$.

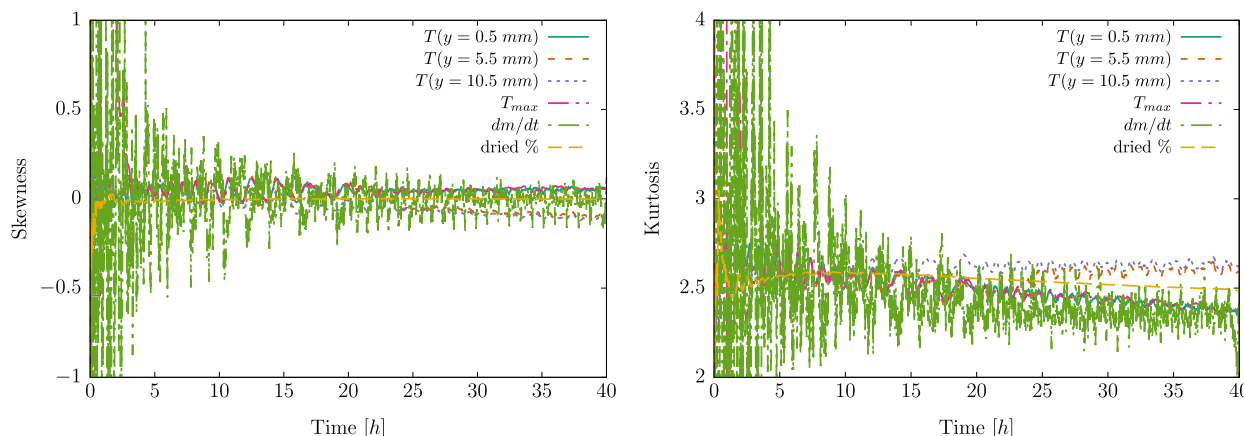


Fig. 10. Time traces of skewness (left) and kurtosis (right) during the primary drying phase.

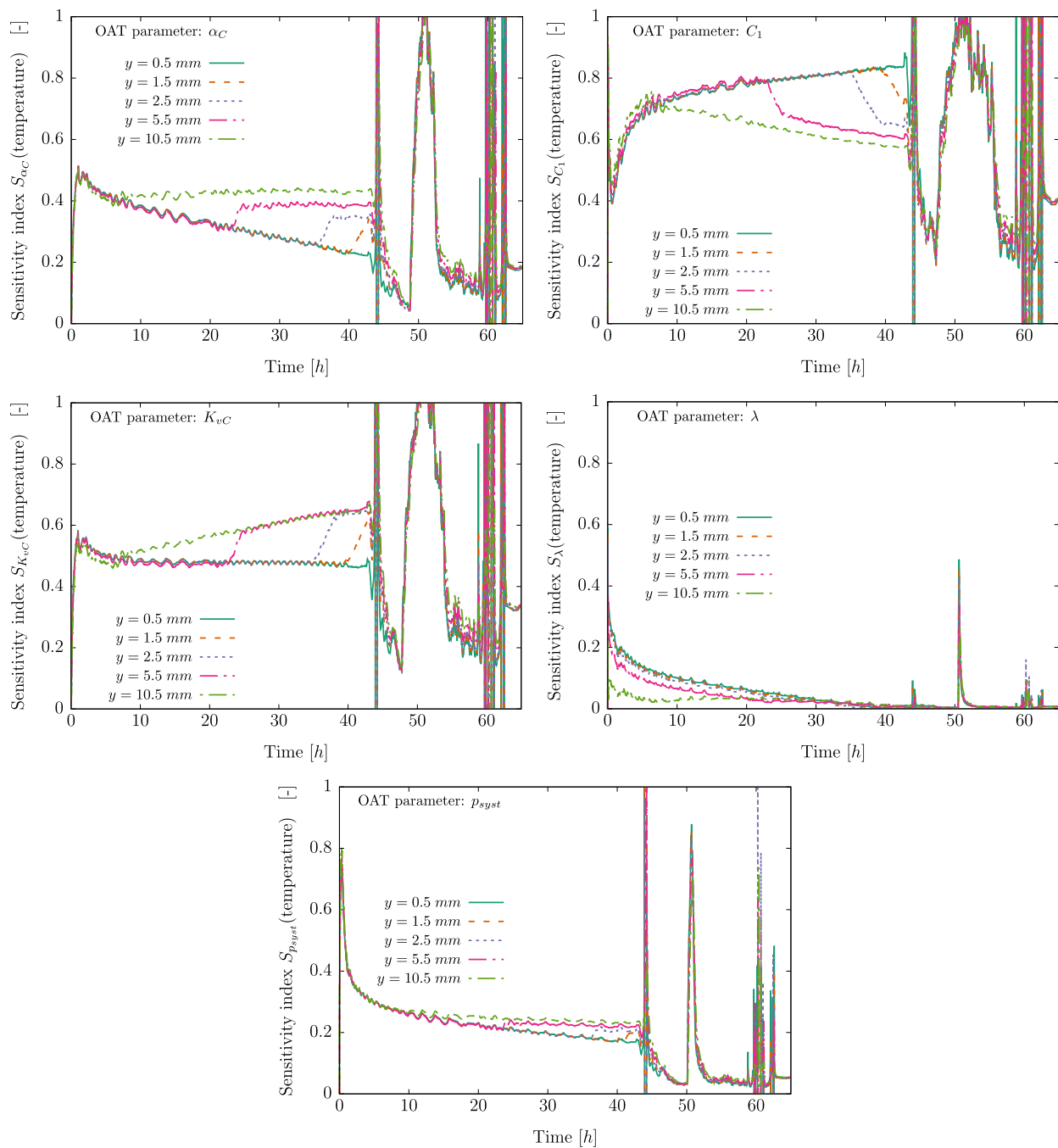


Fig. 11. Sensitivity index for temperature at different position in the vial. Passage of the sublimation front can be clearly observed when looking at the α_C , C_1 and K_{vC} charts.

to be the most influential mass transfer model parameter, and since its value depends to a large extent on the porous structure of the cake, which is a consequence of the material properties and the protocol of the freezing process, it is strongly advised to perform at least one experimental lyophilisation run in order to establish its correct value for the case under consideration. Finally, when the mass flux starts to decrease and only the secondary drying effects remain in the porous cake, the sensitivity of the process is comparable for both heat and mass transfer. The use of the Stochastic Collocation Method for uncertainty studies is very convenient, because the deterministic model is executed many times, and statistical quantities are estimated only by the analysis of the results of deterministic simulations. The deterministic model can be used as a black box, so that the method can be used in conjunction with

any existing mathematical model. The only drawback is the need for a large number of evaluations of the deterministic model. Even though the number of evaluations required by the SCM is much lower than when using the Monte Carlo approach, this still limits the complexity of the deterministic model. As a full 3D Computational Fluid Dynamics simulation of the complete batch coupled with computational submodels for each vial is still extremely costly, the presented sensitivity analysis coupled with a computational analysis of the single characteristic vial lyophilisation, offers a time effective alternative already for the determination of the most sensitive parameters in the different steps of the primary and secondary drying stages, and is, thus, a valuable aid in the planning of the experimental trials, as well as in the construction of a suitable mathematical model for the numerical investigation of the

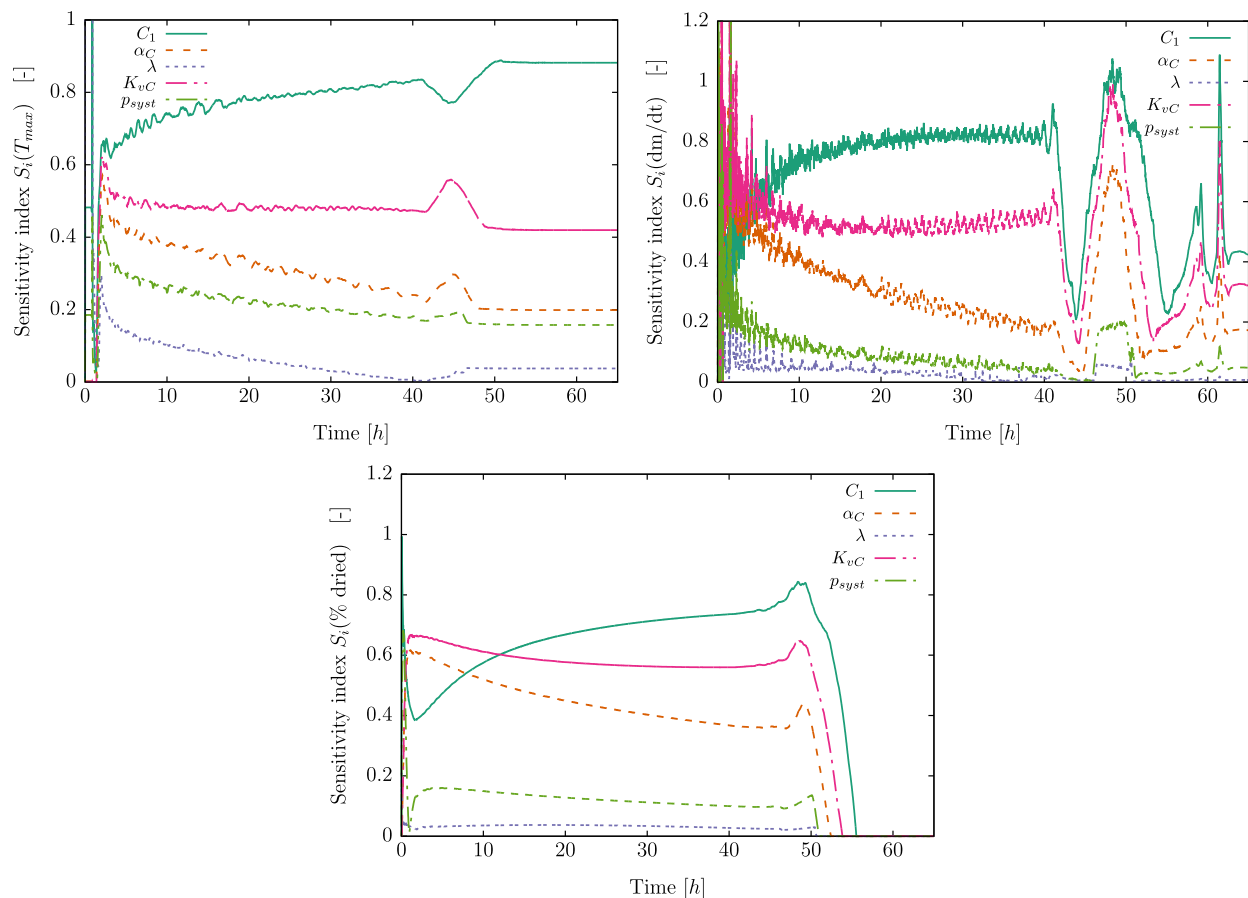


Fig. 12. Sensitivity index for maximal temperature, mass flux and dried material fraction.

design space.

Acknowledgements

Authors acknowledge the financial support from the Slovenian Research Agency (research core funding No. P2-0196).

References

- [1] M.J. Pikal, M.L. Roy, S. Shah, Mass and heat transfer in vial freeze-drying of pharmaceuticals: Role of the vial, *J. Pharm. Sci.* 73 (1984) 1224–1237.
- [2] V.R. Koganti, E.Y. Shalae, M.R. Berry, T. Osterberg, M. Youssef, D.N. Hiebert, F. A. Kanka, M. Nolan, R. Barrett, G. Scalzo, G. Fitzpatrick, N. Fitzgibbon, S. Luthra, L. Zhang, Investigation of design space for freeze-drying: use of modeling for primary drying segment of a freeze-drying cycle, *AAPS PharmSciTech* 12 (2011) 854–861.
- [3] A. Giordano, A.A. Barresi, D. Fissore, On the use of mathematical models to build the design space for the primary drying phase of a pharmaceutical lyophilization process, *J. Pharm. Sci.* 100 (2011) 311–324.
- [4] D. Fissore, R. Pisano, A.A. Barresi, Advanced approach to build the design space for the primary drying of a pharmaceutical freeze-drying process, *J. Pharm. Sci.* 100 (2011) 4922–4933.
- [5] fish 0,punct]">M.J. Millman, A.I. Liapis, J.M. Marchello, An analysis of the lyophilization process using a sorption-sublimation model and various operational policies, *AIChE J.* 31 (1985) 1594–1604.
- [6] P. Sheehan, A.I. Liapis, Modeling of the primary and secondary drying stages of the freeze drying of pharmaceutical products in vials: Numerical results obtained from the solution of a dynamic and spatially multi-dimensional lyophilization model for different operational policies, *Biotechnol. Bioeng.* 60 (1998) 712–728.
- [7] C.S. Song, J.H. Nam, C.-J. Kim, S.T. Ro, A finite volume analysis of vacuum freeze drying processes of skim milk solution in trays and vials, *Drying Technol.* 20 (2002) 283–305.
- [8] S.A. Velardi, A.A. Barresi, Development of simplified models for the freeze-drying process and investigation of the optimal operating conditions, *Chem. Eng. Res. Des.* 86 (2008) 9–22.
- [9] N. Daraoui, P. Dufour, H. Hammouri, A. Hottot, Model predictive control during the primary drying stage of lyophilisation, *Control Eng. Practice* 18 (2010) 483–494.
- [10] M. Ramsak, M. Zdravec, J. Ravnik, J. Iljaz, M. Avanzo, K. Kocevar, S. Irman, M. Cegnar, I. Golobic, A. Sitar, M. Hribersek, Numerical and experimental modeling of lyophilization of lactose and mannitol water solutions in vials, *Computat. Thermal Sci.* (2020), <https://doi.org/10.1615/ComputThermalSci.2020026393>.
- [11] S.T. Mortier, P.J. Van Bockstal, J. Corver, I. Nopens, K.V. Gernaey, T. De Beer, Uncertainty analysis as essential step in the establishment of the dynamic Design Space of primary drying during freeze-drying, *Eur. J. Pharm. Biopharm.* 103 (2016) 71–83.
- [12] P.J. Van Bockstal, S.T. Mortier, J. Corver, I. Nopens, K.V. Gernaey, T. De Beer, Quantitative risk assessment via uncertainty analysis in combination with error propagation for the determination of the dynamic Design Space of the primary drying step during freeze-drying, *Eur. J. Pharm. Biopharm.* 121 (2017) 32–41.
- [13] D. Xiu, Fast numerical methods for stochastic computations: a review, *Commun. Comput. Phys.* 5 (2009) 242–272.
- [14] J. Bai, G. Zhang, D. Wang, A.P. Duffy, L. Wang, Performance comparison of the SGM and the SCM in EMC simulation, *IEEE Trans. Electromagn. Compat.* 58 (2016) 1739–1746.
- [15] L. Mathelin, M.Y. Hussaini, A Stochastic Collocation Algorithm for Uncertainty Analysis, Technical Report February, NASA STI Report Series, NASA/CR-2003-212153, 2003.
- [16] D. Poljak, S. Sesnic, M. Cvetkovic, A. Susnjara, H. Dodig, S. Lalléchère, K. El Khamlichi Drissi, Stochastic collocation applications in computational electromagnetics, *Mathe. Probl. Eng.* (2018) 1–13.
- [17] I. Babuska, F. Nobile, R. Tempone, A stochastic collocation method for elliptic partial differential equations with random input data, *SIAM Rev.* 52 (2010) 317–355.
- [18] S. Bosca, D. Fissore, M. Demichela, Risk-based design of a freeze-drying cycle for pharmaceuticals, *Ind. Eng. Chem. Res.* 54 (2015) 12928–12936.
- [19] J.M. Goldman, H.T. More, O. Yee, E. Borgeson, B. Remy, J. Rowe, V. Sadineni, Optimization of primary drying in lyophilization during early-phase drug development using a definitive screening design with formulation and process factors, *J. Pharm. Sci.* 107 (2018) 2592–2600.
- [20] N. Adhikari, T. Zhu, F. Jameel, T. Tharp, S. Shang, A. Alexeenko, Sensitivity study to assess the robustness of primary drying process in pharmaceutical lyophilization, *J. Pharm. Sci.* 109 (2020) 1043–1049.
- [21] J.M. Goldman, X. Chen, J.T. Register, V. Nesarikar, L. Iyer, Y. Wu, N. Mugheirbi, J. Rowe, Representative scale-down lyophilization cycle development using a seven-vial freeze-dryer (MicroFD), *J. Pharm. Sci.* 108 (2019) 1486–1495.

- [22] M. Bjelošević, K. Bolko Seljak, U. Trstenjek, M. Logar, B. Brus, P. Ahlin Grabnar, Aggressive conditions during primary drying as a contemporary approach to optimise freeze-drying cycles of biopharmaceuticals, *Eur. J. Pharm. Sci.* 122 (2018) 292–302.
- [23] J. Ravnik, I. Golobič, A. Sitar, M. Avanzo, Š. Irman, K. Kočevar, M. Cegnar, M. Zdravec, M. Ramsak, M. Hriberšek, Lyophilization model of mannitol water solution in a laboratory scale lyophilizer, *J. Drug Deliv. Sci. Technol.* 45 (2018).
- [24] www.kambic.com, Kambič, laboratory and process equipment, 2018.
- [25] A.A. Barresi, R. Pisano, D. Fissore, V. Rasetto, S.A. Velardi, A. Vallan, M. Parvis, M. Galan, Monitoring of the primary drying of a lyophilization process in vials, *Chem. Eng. Process.* 48 (2009) 408–423.
- [26] M. Ramsak, J. Ravnik, M. Zdravec, M. Hriberšek, J. Iljaž, Freeze-drying modeling of vial using BEM, *Eng. Anal. Boundary Elem.* 77 (2017) 145–156.
- [27] H. Sadikoglu, A.I. Liapis, Mathematical modelling of the primary and secondary drying stages of bulk solution freeze-drying in trays: parameter estimation and model discrimination by comparison of theoretical results with experimental data, *Drying Technol.* 15 (1997) 791–810.
- [28] N. Vorhauer-Huget, D. Mannes, M. Hilmer, S. Gruber, M. Strobl, E. Tsotsas, P. Foerst, Freeze-drying with structured sublimation fronts—visualization with neutron imaging, *Processes* 8 (2020) 1091.
- [29] A. Sitar, K. Škrlec, J. Voglar, M. Avanzo, K. Kočevar, M. Cegnar, Š. Irman, J. Ravnik, M. Hriberšek, I. Golobič, Effects of controlled nucleation on freeze-drying lactose and mannitol aqueous solutions, *Drying Technol.* 36 (2017) 1263–1272.
- [30] P. Foerst, T. Melo de Carvalho, M. Lechner, T. Kovacevic, S. Kim, C. Kirse, H. Briesen, Estimation of mass transfer rate and primary drying times during freeze-drying of frozen maltodextrin solutions based on x-ray μ -computed tomography measurements of pore size distributions, *J. Food Eng.* 260 (2019) 50–57.
- [31] A.K. Konstantinidis, W. Kuu, L. Otten, S.L. Nail, R. Sever, Controlled nucleation in freeze-drying: effects on pore size in the dried product layer, mass transfer resistance, and primary drying rate, *J. Pharm. Sci.* 100 (2011) 3453–3470.
- [32] A.A. Barresi, V. Rasetto, D.L. Marchisio, Use of computational fluid dynamics for improving freeze-dryers design and process understanding. part 1: Modelling the lyophilisation chamber, *Eur. J. Pharm. Biopharm.* 129 (2018) 30–44.
- [33] A.A. Barresi, D.L. Marchisio, Computational fluid dynamics data for improving freeze-dryers design, *Data Brief* 19 (2018) 1181–1213.
- [34] B. Scutella, S. Passot, E. Bourles, F. Fonseca, I.C. Trelea, How vial geometry variability influences heat transfer and product temperature during freeze-drying, *J. Pharm. Sci.* 106 (2017) 770–778.
- [35] M. Brülls, A. Rasmuson, Heat transfer in vial lyophilization, *Int. J. Pharm.* 246 (2002) 1–16.
- [36] B. Scutella, A. Plana-Fattori, S. Passot, E. Bourles, F. Fonseca, D. Flick, I. Trelea, 3d mathematical modelling to understand atypical heat transfer observed in vial freeze-drying, *Appl. Therm. Eng.* 126 (2017) 226–236.
- [37] T. Zhu, E.M. Moussa, M. Witting, D. Zhou, K. Sinha, M. Hirth, M. Gastens, S. Shang, N. Nere, S. Chetan, A. Alexeenko, F. Jameel, Predictive models of lyophilization process for development, scale-up/tech transfer and manufacturing, *Eur. J. Pharm. Biopharm.* 128 (2018) 363–378.
- [38] M.J. Pikal, R. Bogner, V. Mudhivartha, P. Sharma, P. Sane, Freeze-drying process development and scale-up: scale-up of edge vial versus center vial heat transfer coefficients, *K.v. J. Pharm. Sci.* 105 (2016) 3333–3343.
- [39] S. Smolyak, Quadrature and interpolation formulas for tensor products of certain classes of functions, *Soviet Math. Dokl.* 4 (1963) 240–243.
- [40] V. Barthelmann, E. Novak, K. Ritter, High dimensional polynomial interpolation on sparse grids, *Adv. Comput. Mathe.* 12 (2000) 273–288.
- [41] F. Nobile, R. Tempone, C.G. Webster, A sparse grid stochastic collocation method for partial differential equations with random input data, *SIAM J. Num. Anal.* 46 (2008) 2309–2345.
- [42] M. Stoyanov, User Manual: TASMANIAN Sparse Grids, Technical Report ORNL/TM-2015/596, Oak Ridge National Laboratory, One Bethel Valley Road, Oak Ridge, TN, 2015.
- [43] M.K. Stoyanov, C.G. Webster, A dynamically adaptive sparse grids method for quasi-optimal interpolation of multidimensional functions, *Comput. Mathe. Appl.* 71 (2016) 2449–2465.
- [44] A. Saltelli, M. Ratto, T. Andres, F. Campolongo, D. Gatelli, M. Saisana, S. Tarantola, *Global Sensitivity Analysis: The Primer*, John Wiley and Sons Ltd, West Sussex, England, 2008.
- [45] S.M. Patel, T. Doen, M.J. Pikal, Determination of end point of primary drying in freeze-drying process control, *AAPS PharmSciTech* 11 (2010) 73–84.